isvr Institute of Sound and Vibration Research

Equipment Isolation of a SDOF System with an Inertial Acutator using Double Feedback Control Strategies

L. Benassi, P. Gardonio and S.J. Elliott

ISVR Technical Memorandum No 893

October 2002

University of Southampton

SCIENTIFIC PUBLICATIONS BY THE ISVR

Technical Reports are published to promote timely dissemination of research results by ISVR personnel. This medium permits more detailed presentation than is usually acceptable for scientific journals. Responsibility for both the content and any opinions expressed rests entirely with the author(s).

Technical Memoranda are produced to enable the early or preliminary release of information by ISVR personnel where such release is deemed to the appropriate. Information contained in these memoranda may be incomplete, or form part of a continuing programme; this should be borne in mind when using or quoting from these documents.

Contract Reports are produced to record the results of scientific work carried out for sponsors, under contract. The ISVR treats these reports as confidential to sponsors and does not make them available for general circulation. Individual sponsors may, however, authorize subsequent release of the material.

UNIVERSITY OF SOUTHAMPTON

INSTITUTE OF SOUND AND VIBRATION RESEARCH

SIGNAL PROCESSING AND CONTROL GROUP

Equipment Isolation of a SDOF System with an Inertial Actuator using Double Feedback Control Strategies

by

L. Benassi, P. Gardonio and S. J. Elliott

ISVR Technical Memorandum No. 893

October 2002

Authorised for issue by
Prof S J Elliott
Group Chairman

ABSTRACT

Vibration isolators are required to protect a delicate piece of equipment from the vibration of a structure to which it is attached. This report describes a theoretical investigation into an active vibration isolation system in which an electromagnetic inertial actuator is installed on top of a piece of equipment which is connected to a vibrating plate through a passive mount. Double feedback control schemes are discussed, and simulation results are reported.

For each case subject of this study, the stability region and the ability to minimize the equipment velocity are discussed. It is shown that a phase-lag compensator within the internal control loop and an external velocity feedback control loop offer a very promising solution both in terms of stability of and performance of the system.

TABLE OF CONTENTS

1. INTRODUCTION

Isolators are generally required to protect a piece of delicate equipment in a severe vibration environment. Using passive mounts there is a trade-off between low and high frequency isolation performances depending on the damping of the mount, as described by Crede and Ruzicka (1996).
To provide a more favourable static and dynamic stiffness compromise, active isolation solutions must be used, which are usually based on mounts and actuators.

Actuators are used in active vibration control to generate a secondary vibrational response, and in practice they can be configured either to react off the base structure or function as an inertial actuator (also called proof-mass actuator). Inertial actuators do not need to react off a base structure, so they can be used as modules that can be directly installed on a vibrating structure. This feature makes them very attractive. This was investigated by Elliott *et al.*, (2001), and Benassi *et al.*, (2002a). It was found that the design of a feedback controller based on inertial actuators involves a trade-off between performance (the attenuation of the disturbance) and robust stability (the ability to remain stable under changing conditions). In particular, different strategies for active isolation using an inertial actuator were studied. Once the theoretical analysis was completed, a realistic case using real commercial components (Ananthaganeshan *et al.*, 2002) was analysed.
It was found that while single loop feedback control strategies such as velocity feedback, integrated velocity feedback, force feedback and integrated force feedback often offer severe limitations both in terms of stability and performance, double loop feedback control strategies based on a combination of the above show very promising results.

This report deals with the stability and performance analysis of a single degree of freedom system, composed of a piece of equipment, which is mounted on a vibrating plate through a mount. Double active feedback control strategies are implemented through an inertial actuator and a couple of sensors. The objective of this work is to investigate feedback control strategies in order to minimize the equipment velocity over a wide bandwidth (Active Vibration Isolation).

2. ACTIVE ISOLATION OF A LUMPED MASS EQUIPMENT MOUNTED ON A VIBRATING PLATE VIA A SPRING-DASHPOT MOUNT

In this study, a matrix model has been used which assumes that the system is divided into four elements: the vibrating plate, the passive mount, the equipment, and the inertial actuator. The dynamics of each of these elements is evaluated using mobility functions. Figure 1 shows the typical system that has been used in this study and the numerical values assumed for the simulations. With these values the actuator has a natural frequency of about 10 Hz and a damping ratio of about ζ=4.5%, the equipment mounting system has a natural frequency of about 21.5 Hz and a damping ratio of about ζ=5.2%, and the vibrating base has a first natural frequency of about 44.8 Hz and a damping ratio of about ζ=4.8%.

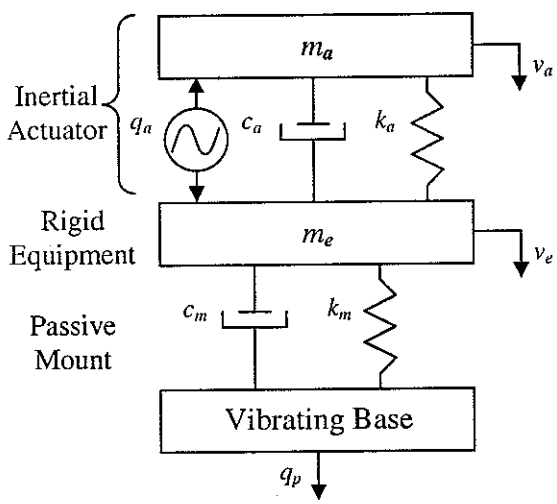

m_a = Inertial Actuator Dynamic Mass = 0.91 Kg
c_a = Inertial Actuator Damping Factor = 5.8 Ns/m
k_a = Inertial Actuator Spring Stiffness = 3900 N/m
m_e = Equipment Mass = 1.08 Kg
c_m = Passive Mount Damping Factor = 18 Ns/m
k_m = Passive Mount Spring Stiffness = 20000 N/m

The mechanical properties of the vibrating plate, which is a steel plate with two clamped edges and two free edges, are fully described by Gardonio *et al.* (1997a)

q_p = Primary Force (disturbance)
q_a = Secondary Force (control)
v_a = Inertial Actuator Velocity
v_e = Equipment Velocity

Figure 1 *Schematic of a vibration isolation system with an inertial actuator.*

Details of the mobilities and impedances used to describe the system throughout this work can be found in Benassi *et al.* (2002b), while Appendix A describes the sign conventions and the complete model equations. In particular, we are interested in the behaviour of the inertial actuator, whose schematic is shown in Figure 2. q_t is the total transmitted force underneath and it can be expressed as a function of the control force and the equipment velocity as follows

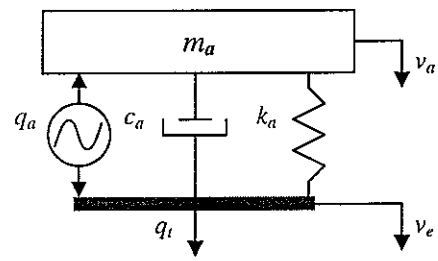

Figure 2 *Schematic and sign convention of an inertial actuator.*

$$q_t = \frac{-\omega^2 m_a}{k_a + j\omega c_a - \omega^2 m_a} q_a - \frac{j\omega m_a k_a - \omega^2 m_a c_a}{k_a + j\omega c_a - \omega^2 m_a} v_e \tag{1}$$

or, in a more compact expression

$$q_t = G q_a - Z_{open} v_e \tag{2}$$

where G can be regarded as the blocked actuator response, and Z_{open} as the open loop impedance of the passive components of the inertial actuator.

The magnitude and phase of the blocked actuator response is plotted in Figure 3(a) from which it can be seen that q_t/q_a is negative at low frequency. In fact, when q_a is positive (the actuator mass is expanding), the passive components within the actuator (spring and damper) are expanded and therefore they generate a force which tends to restore the system to its natural condition. Given the sign convention described above, this force is equal to $-q_t$. Also, it can be seen that q_t tends to q_a for $\omega >> \omega_a$, where $\omega_a = \sqrt{k_a / m_a}$.

The magnitude and phase of the frequency response of the passive components of the inertial actuator is shown in Figure 3(b), in which it can be seen that the real part is always greater than zero (passive behaviour).

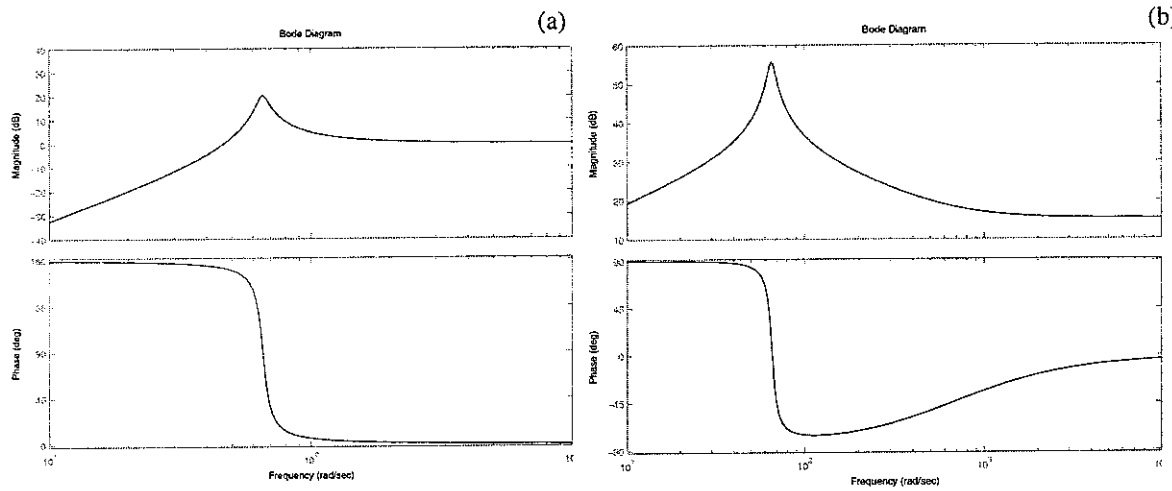

Figure 3 *Magnitude and phase of the blocked frequency response of the inertial actuator (a), and magnitude and phase of the frequency response of the passive components of the inertial actuator (Z_{open} in Equation (2)).*

2.1 Inner Loop: Force Feedback Control

Given the inertial actuator, when force feedback control is implemented, the schematic is shown in Figure 4. The total transmitted force q_t is measured and fed back to the inertial actuator through a constant real positive gain $H(j\omega)=h$. The command signal f_c can be considered, in control terms, as the reference point. It will be used when the outer loop is implemented, but understanding its role is essential at this stage.

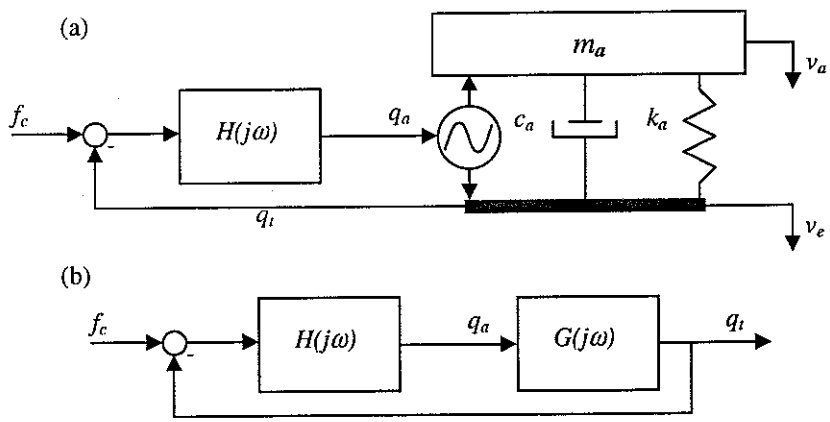

Figure 4 *Schematic of an inertial actuator and implementation of the inner total transmitted force feedback control (a), and equivalent block diagram (b).*

The Nyquist plot of the blocked actuator response is shown in Figure 5. The stability analysis of such a system plays an important role in the discussion about whether force and velocity feedback control is a good solution to the equipment isolation problem. At low frequency, the Nyquist plot lies very close to the critical point and therefore instability is likely to happen especially to real systems where an additional phase shift is present due to the electronic components. In sum, from a stability point of view, the force and velocity controller raises some concerns and special attention must be paid when real systems are implemented. This is mainly due to the fact that even under ideal conditions, at low frequency the overall system works close to its stability limit.

It can also be noted that at high frequency the plot does not go to the origin and this is due to the fact that at high frequency the magnitude in the corresponding Bode plot (Figure 3(a)) is constant.

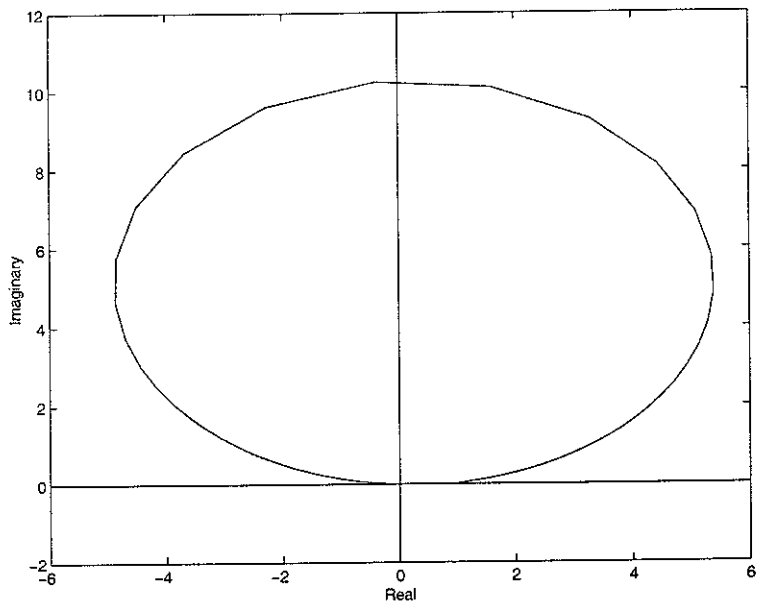

Figure 5 *Nyquist plot of the blocked actuator response described in equation (1).*

The secondary force (control signal to the inertial actuator) is given by

$$q_a = h(f_c - q_t) \tag{3}$$

which, substituted into (2), provides the closed loop total transmitted force as a function of the command signal and the equipment velocity. This is given by

$$q_t = \frac{Z_{open}}{1+Gh} f_c + \frac{Gh}{1+Gh} v_e \tag{4}$$

When the single terms are expanded, the expression becomes

$$q_t = \frac{-\omega^2 m_a h}{k_a + j\omega c_a - \omega^2 m_a (1+h)} f_c - \frac{j\omega m_a k_a - \omega^2 m_a c_a}{k_a + j\omega c_a - \omega^2 m_a (1+h)} v_e \tag{5}$$

which can be grouped as

$$q_t = A_1 f_c - B_1 v_e \tag{6}$$

The total transmitted force q_t per unit control command f_c is plotted in Figure 6(a). When the gain h increases, the total transmitted force tends to the control command. This means that using the outer control loop it is possible to transmit all the desired force to the equipment. In fact, it should be noted from equation (4) that $Z_{closed} = \frac{Z_{open}}{1+GH} << Z_{open}$ and if $GH >> 1$ then $q_t \cong f_c$, which means that the total transmitted force can be regulated using the command signal f_c.

A second important aspect is that, when the gain h increases, the actuator resonance is shifted to lower frequencies, while its magnitude increases, getting closer to the unstable region. This was also described by Benassi *et al.* (2002a). In fact, it was found that total transmitted force is proportional to the acceleration of the actuator. Hence, force feedback is equivalent to feeding back the actuator acceleration. This leads to the conclusion that force feedback control has the physical meaning of adding an "apparent" mass to the inertial actuator mass.

In Figure 6(a) the dashed line shows a peak whose magnitude is lower than the peak depicted using the faint line. This is due to a numerical approximation of the software. In reality the former peak should be higher then the latter. This indicates the fact that the inner force feedback loop is able to bring the inertial actuator resonance to lower frequencies, while its magnitude increases, which is an indication of the fact that the system is closer to instability at such low frequency.

Figure 6(b) shows the total transmitted force q_t per unit equipment velocity. Even in this case the resonance frequency shift can be observed, and this implies that when the inner feedback gain h is increased, q_t / v_e tends to zero, which indicates that for high gains the system behaves as if the inertial actuator is no longer present. In general though, for reasonable values of h, the magnitude of q_t / v_e is much lower if compared to the uncontrolled case.

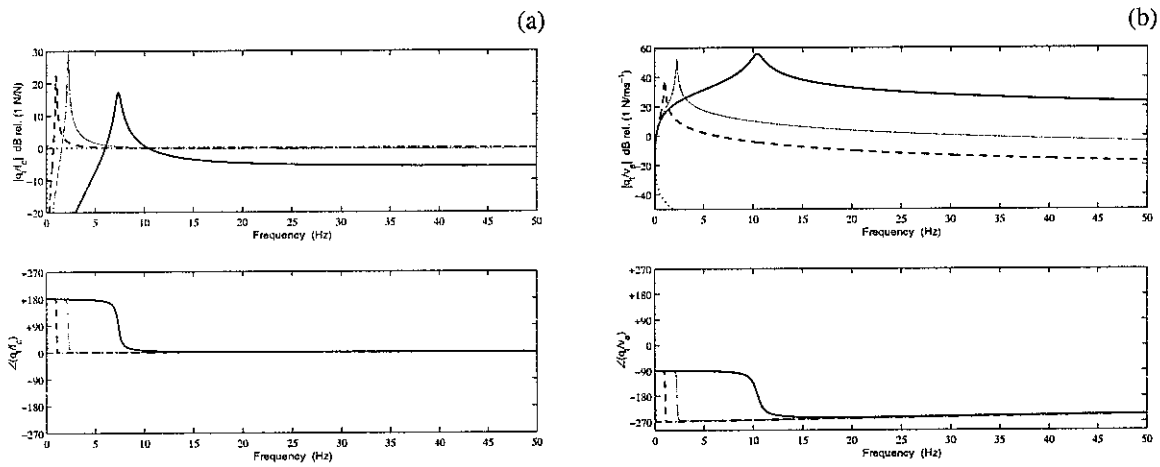

Figure 6 *(a): Total transmitted force per unit control command when different inner loop gains h in H(jω)=h are used: h=1 (solid), h=20 (faint), h=100 (dashed), and h=100,000 (dotted). (b): Total transmitted force per unit equipment velocity when h=0 (solid), h=20 (faint), h=100 (dashed), and h=100,000 (dotted).*

2.2 Inner Loop: Integrated Force Feedback Control

In Figure 4, if $H(j\omega) = h/(j\omega)$ then integrated force feedback control is implemented. The correspondent Nyquist plot (Figure 7) entirely lies on the positive real axis. This is due to the effect of the integration on the plot in Figure 5. As a result, that plot is rotated by 90° clockwise. Therefore, when the phase lags due to the electronic components are introduced, the overall system remains stable within a large set of gains. In other words, the ideal system is unconditionally stable, thus the integrated force feedback tends to make the overall system more robust.

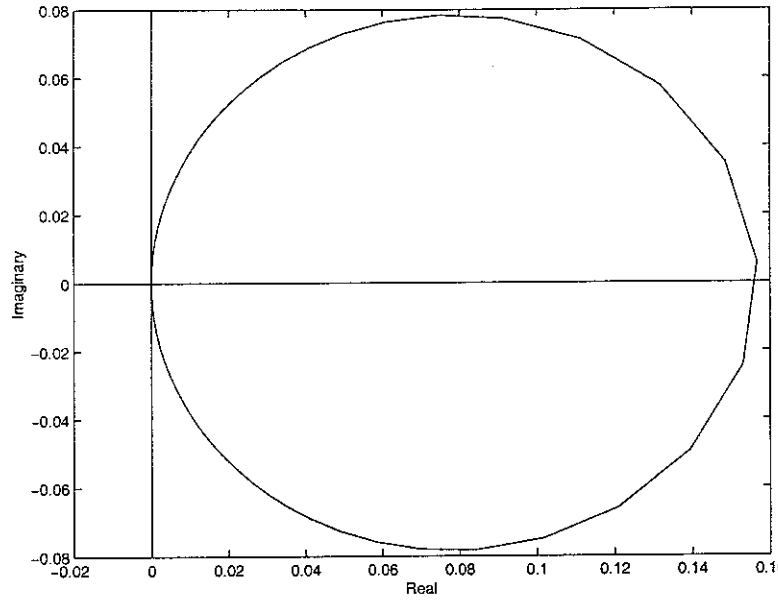

Figure 7 *Nyquist plot of the blocked actuator response when $H(j\omega)=h/j\omega$.*

In this case, the secondary force is given by

$$q_a = h\frac{\omega_0}{j\omega}(f_c - q_t) \tag{7}$$

The control law is written in the form $h\frac{\omega_0}{j\omega}$, so that the gain h is unitless and ω_0=1 rad/s. When (7) is substituted into (1), the total transmitted force becomes

$$q_t = \frac{-\omega^2 m_a h}{k_a + j\omega c_a - \omega^2 m_a + j\omega m_a h} f_c - \frac{j\omega m_a k_a - \omega^2 m_a c_a}{k_a + j\omega c_a - \omega^2 m_a + j\omega m_a h} v_e \tag{8}$$

which can be written in the compact form

$$q_t = A_2 f_c - B_2 v_e \tag{9}$$

The total transmitted force q_t per unit control command f_c is plotted in Figure 8(a). Unlike the previous case, the resonance frequency does not change when the gain increases. On the other hand, q_t tends to f_c when very high gains are implemented. For reasonable values though, the magnitude decays past the resonance frequency and a phase shift occurs. Compared to the force feedback control in which q_t tends to f_c as well, here the magnitude

assumes lower levels, which implies that higher h values are needed in this scheme compared to the previous one in order to obtain the same levels of q_t.

Figure 8(b) shows the total transmitted force q_t per unit equipment velocity v_e. When the inner feedback gain h is increased, an attenuation can be noted within the resonance frequency, but at higher frequencies, q_t / v_e decays. In other words, the system becomes so damped that its resonance disappears and it seems that the inertial actuator has been removed.

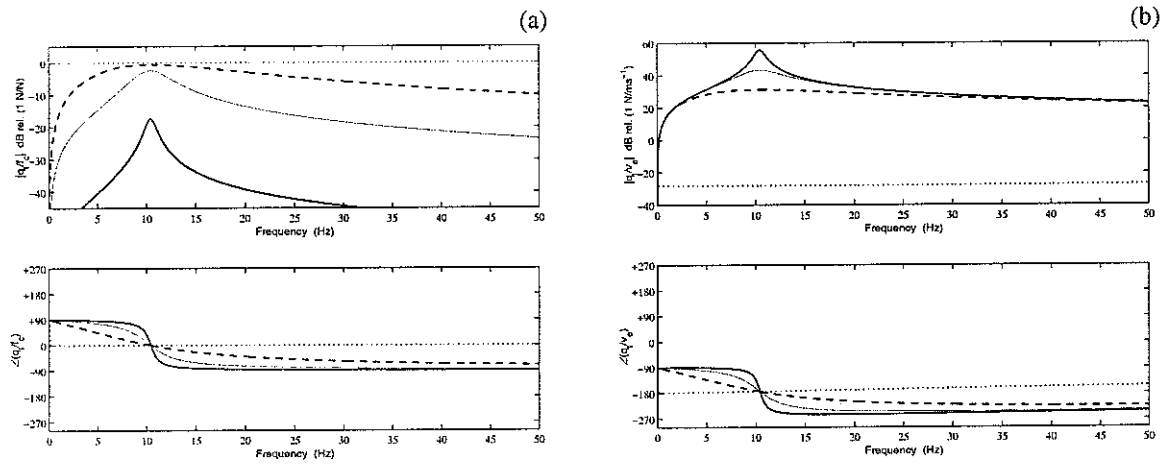

Figure 8 *(a): Total transmitted force per unit control command when different inner loop gains h in $H(j\omega)=h/j\omega$ are used: h=1 (solid), h=20 (faint), h=100 (dashed), and h=100,000 (dotted). (b): Total transmitted force per unit equipment velocity when h=0 (solid), h=20 (faint), h=100 (dashed), and h=100,000 (dotted).*

An intermediate scheme based on the measurement of the integrated total transmitted force to the equipment was also analysed. The inner feedback gain $H(j\omega)$ was chosen to be a positive real constant h. The Nyquist plot is shown in Figure 7 and the total transmitted force per unit equipment velocity is shown in Figure 8(b). Unlike the other schemes, the total transmitted force per unit control command f_c shows the weakness of this strategy. In fact, for very high values of the gain h , q_t / f_c tends to h, but when h assumes reasonable values, q_t / f_c tends to $j\omega$, which means that it is frequency dependent. For this reason, the implementation of this feedback control scheme is not recommended.

From a stability point of view, the force feedback control scheme does not guarantee a good stability margin at low frequency. This is especially true when the outer velocity gain is increased. In addition, when real electronic components are added to the ideal system, the stability margin rapidly decreases and the overall system falls very close towards the unstable region. On the other hand, from a performance point of view, this scheme offers very good results using lower power than the other schemes.

When an integrator is added to the system, the overall system significantly improves its stability characteristics. This can be noted in the Nyquist plot, which is rotated by 90° clockwise. On the other hand, if high performance is needed, very high gains are necessary and therefore a lot of power is consumed. At the same time, using these latter schemes, attenuation over a large bandwidth is possible.

The idea is then to alter the inner loop in such a way that it behaves like a force and velocity feedback controller at frequencies higher than a certain appropriate value, which will be discussed in the next section and it behaves like an integrated force and velocity feedback controller at low frequencies. By doing so, the system will preserve high stability characteristics at low frequency and will also preserve good performance at high frequency, which will be obtained using relatively low energy levels.

All these aspects will be discussed in the next sections.

2.3 Inner Loop: Phase-lag Compensator

In Figure 4, if $H(j\omega) = h'\frac{j\omega + \omega_1}{j\omega}$ then the correspondent Nyquist plot is shown in Figure 9. It can be noted that the behaviour of the closed loop system from a stability point of view is in between the behaviour of the previous two cases. In particular, at low frequency the closed loop system is almost as robust as the integrated force feedback case.

A detailed discussion on the appropriate choice of ω_l is given in Appendix B. It is shown that the choice of ω_l becomes of critical importance in order to assess a reasonable trade-off between stability of the overall system (especially at low frequency) and its performance. In fact, when ω_l is small, the system behaves similarly to the force and velocity implementation scheme. On the other hand, when ω_l is chosen to be large then stability problems are likely to happen at higher frequencies.

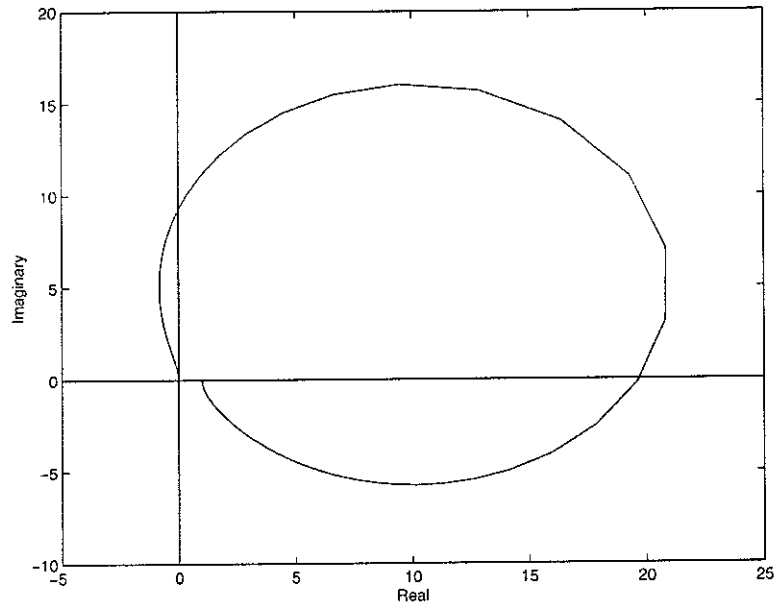

Figure 9 *Nyquist plot of the blocked actuator response when the phase-lag compensator is implemented.*

The control law is written in the form $h'\frac{j\omega+\omega_1}{j\omega}$, so that the gain h' is unitless and $\omega_1=2\pi 22=138.16$ rad/s. In order to make h' comparable to the gains described in the previous sections, it is necessary that

$$h'=\frac{h}{\omega_1} \tag{10}$$

The secondary force is given by

$$q_a = h'\frac{j\omega+\omega_1}{j\omega}(f_c - q_t) \tag{11}$$

Substituting equation (11) into (1), the total transmitted force becomes

$$\begin{aligned} q_t = & \frac{-\omega^2 m_a h' + j\omega m_a h'\omega_1}{k_a + j\omega c_a - \omega^2 m_a(1+h') + j\omega m_a h'\omega_1} f_c \\ & - \frac{j\omega m_a k_a - \omega^2 m_a c_a}{k_a + j\omega c_a - \omega^2 m_a(1+h') + j\omega m_a h'\omega_1} v_e \end{aligned} \tag{12}$$

which can be written in the compact form

$$q_t = A_3 f_c - B_3 v_e \tag{13}$$

Figure 10(a) shows the total transmitted force to the equipment per unit control force. As the gain h increases, q_t tends to f_c at all frequencies. Compared to the previous scheme (Figure 8(a)), at frequencies higher than the resonance, the magnitude is steadier, indicating a better performance at high frequency since q_t is closer to f_c than in the previous case. Also, unlike the previous case, there is no phase lag at frequencies higher than the resonance.

Figure 10(b) shows the total transmitted force per unit equipment velocity. When the gain h increases, q_t / v_e tends to zero, but this is actually achieved for very large values of the gain. Otherwise, the behaviour is similar to the previous case. Compared to the uncontrolled case (solid line), when the controller is activated the first resonance is no longer present in the q_t / v_e equation. This can be physically explained considering the fact that when the gain h in the phase-lag compensator increases, the closed loop system tends to an equivalent system in which the inertial activator has been removed.

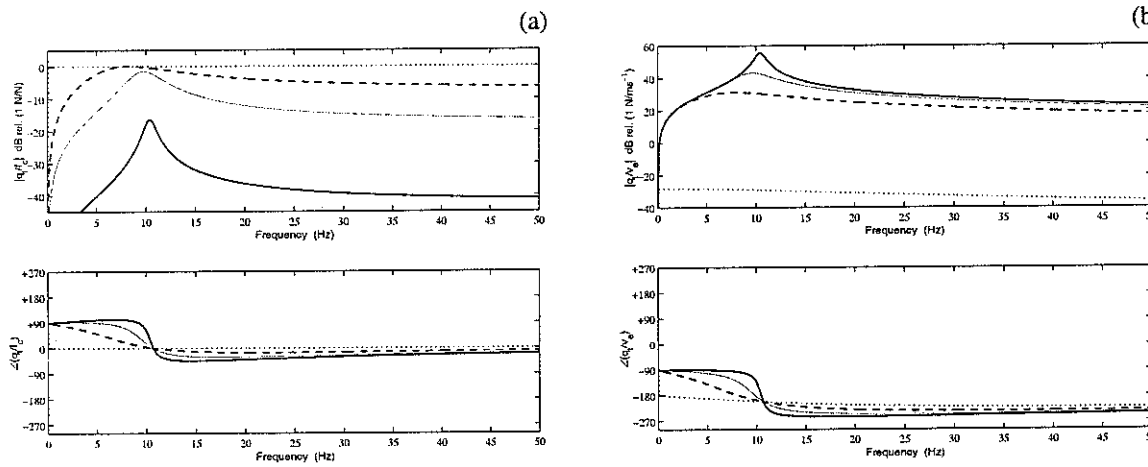

Figure 10 *(a): Total transmitted force per unit control command when different inner loop gains h in the phase-lag compensator are used: h=1 (solid), h=20 (faint), h=100 (dashed), and h=100,000 (dotted). (b): Total transmitted force per unit equipment velocity when h=0 (solid), h=20 (faint), h=100 (dashed), and h=100,000 (dotted).*

2.4 Outer Loop: Force Feedback and Velocity Feedback Control

Figure 11 shows the schematic of the entire system when the inner loop is implemented.

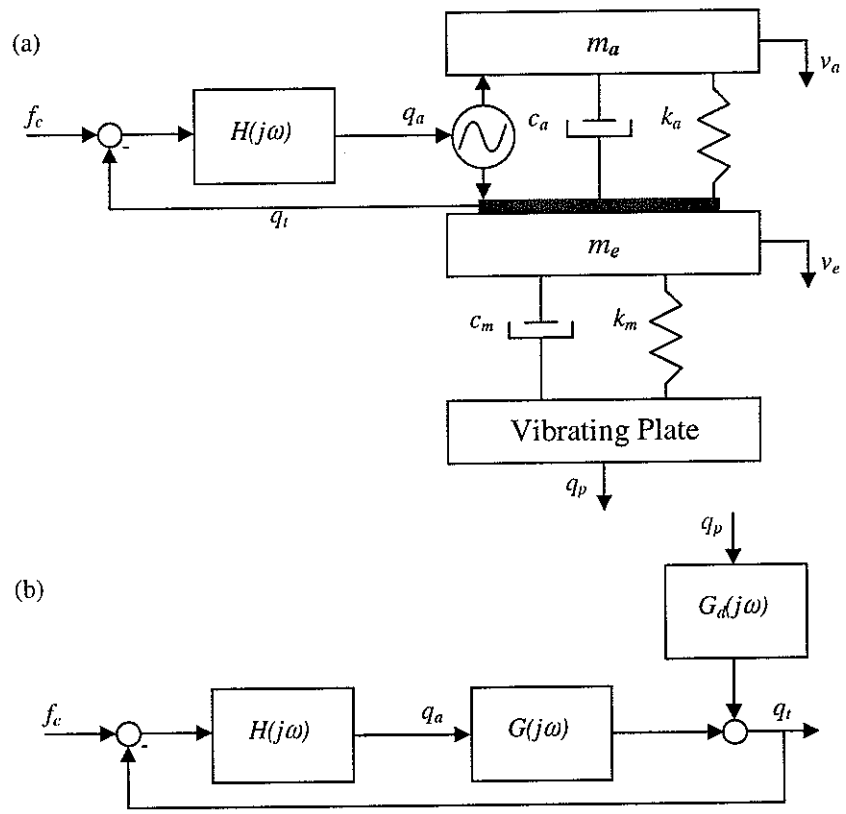

Figure 11 *Schematic of a vibration isolation system with an inertial actuator and implementation of the inner total transmitted force feedback control (a), and equivalent block diagram (b).*

Since the objective of this work is to minimize the equipment velocity, the analytical expression for the equipment velocity as a function of the primary force q_p and the total transmitted force q_t was obtained:

$$v_e = \frac{Y_e Z_m Y_b}{1 + Z_m (Y_e + Y_b)} q_p + \frac{Y_e (1 + Y_b Z_m)}{1 + Z_m (Y_e + Y_b)} q_t \tag{14}$$

where

$$Y_e = \frac{1}{j\omega m_e} = \text{Mobility of the rigid equipment}$$

$$Y_b = \frac{1}{j\omega m_b + c_b + \frac{k_b}{j\omega}} = \text{Mobility of the vibrating base}$$

$$Z_m = c_m + \frac{k_m}{j\omega} = \text{Impedance of the passive mount}$$

Substituting equation (6) into (14), the expression of the equipment velocity, when the force inner loop is implemented, is given by

$$v_e = \frac{Y_e Z_m Y_b}{1 + Z_m(Y_e + Y_b + Y_e B_1 Y_b) + Y_e B_1} q_p + \frac{Y_e A_1 (1 + Y_b Z_m)}{1 + Z_m(Y_e + Y_b + Y_e B_1 Y_b) + Y_e B_1} f_c \quad (15)$$

Figure 12 shows a schematic of the system when both inner and outer loops are implemented. It can be noted that the outer loop is a velocity feedback control scheme, and it aims to take energy away from the system, through its constant real positive gain Z_D. In particular,

$$f_c = -Z_D v_e \quad (16)$$

Substituting (16) into (15) the equipment velocity per primary force is given by

$$v_e = \frac{Y_e Z_m Y_b}{1 + Z_m(Y_e + Y_b + Y_e B_1 Y_b) + Y_e B_1 + Y_e A_1 (1 + Y_b Z_m) Z_D} q_p \quad (17)$$

Figure 13(a) shows the equipment velocity per unit command signal for different values of the inner loop gain h. Similarly to Figure 13(b), the effect of increasing the equipment velocity and the shift of the first resonance can be noted.

Figure 13(b) shows the equipment velocity per unit primary force for different values of the inner loop gain h. It can be noted that the inner loop causes v_e to increase, but has the beneficial effect of bringing the first resonance to lower frequencies (in particular, see the faint line).

Figure 13(c) shows the Nyquist plot of v_e/f_c, which effectively determines the stability of the closed loop system once the outer velocity feedback control is implemented. When the inner force feedback gain h is increased, considering that the system with the inner control

loop is unconditionally stable (Figure 5), the effect of increasing Z_D is good attenuation and unconditional stability for all frequencies greater than the first resonance, which happens to be at very low frequency. When Z_D increases, the closed loop system behaves as if the velocity feedback loop dominates over the inner loop, therefore the overall system becomes conditionally stable (i.e. for some Z_D greater than a certain value the very low frequency resonance brings the system to instability).

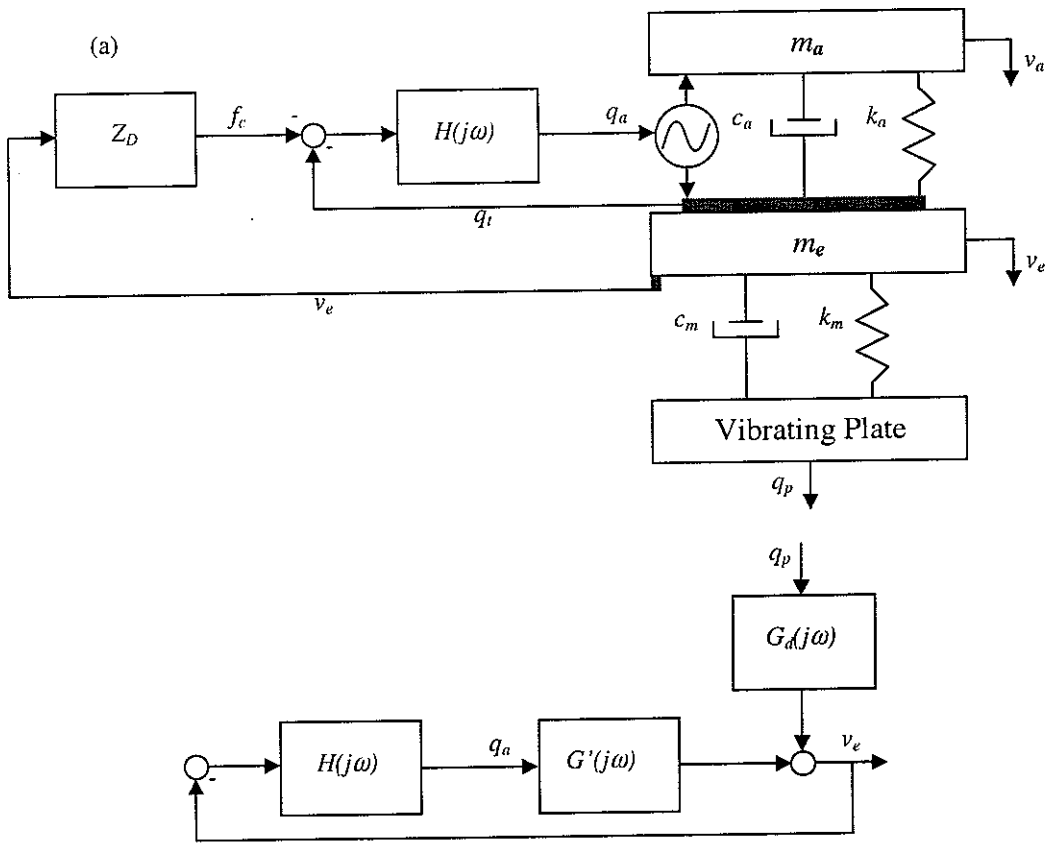

Figure 12 *Schematic of a vibration isolation system with an inertial actuator and implementation of the inner total transmitted force feedback control and the outer velocity feedback control (a), and equivalent block diagram (b).*

However, in order to bring the system to the unstable region, high values for Z_D are needed, much higher than the critical gain that can be experienced using a mere velocity feedback. This latter property is due to the interesting feature of the force and velocity feedback scheme of making stable those systems that were previously unstable. In fact, as

shown in Section 2.1, at low frequency the Nyquist plot lies very close to the critical point and therefore instability is likely to happen especially to real systems where an additional phase shift is present due to the electronic components. It was found (Benassi *et al.*, 2002a) that force feedback control is able to stabilize those systems with velocity feedback that are unstable due to the high velocity gain.

In sum, from a stability point of view, the force and velocity controller raises some concerns and special attention must be paid when real systems are implemented. This is mainly due to the fact that even under ideal conditions, at low frequency the overall system works close to its stability limit.

On the other hand, when the inner gain h assumes reasonably low values, part of the Nyquist plot in Figure 13(c) relative to the first resonance lies within the unit circle centred at (-1,0), which indicates enhancement in the overall closed loop response.

Figure 13(d) shows the equipment velocity per unit primary excitation. The effect of the inner force gain h=100 can be seen from the presence of the shifted first resonance at low frequency. In particular, its magnitude is negligible and its presence can only be noticed from the phase plot. Performance-wise, it is shown that good vibration isolation conditions can be achieved with relatively low gains. Being able to obtain the desired condition spending low energy quantities is important, even if most of the times these conditions are, as explained above, within a narrow stability margin. In conclusion, there is a trade-off between performance and robustness, which makes the force and velocity control scheme very attractive on one hand, but on the other hand it makes it impractical. In fact the problem is that, when the gain h increases, the actuator resonance moves to lower frequencies. In this case, the Nyquist plot of the inner feedback lies, at low frequency, closer to the critical point and therefore in real applications the overall system might become unstable.

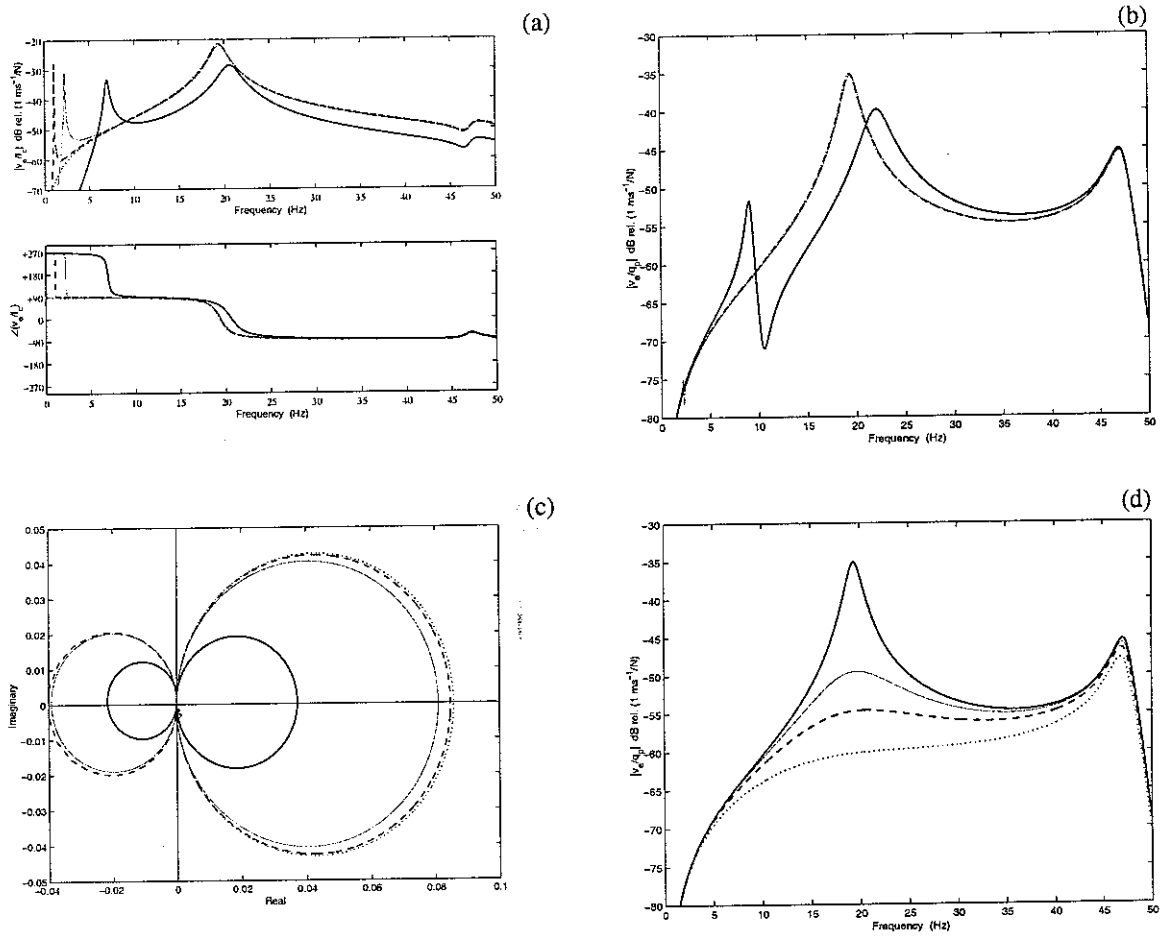

Figure 13 *(a): Equipment velocity per unit command signal when different inner loop gains h in H(jω)=h are used: h=1 (solid), h=20 (faint), h=100 (dashed), and h=100,000 (dotted). (b): Equipment velocity per unit primary force when h=0 (solid), h=20 (faint), h=100 (dashed), and h=100,000 (dotted). (c): Nyquist plot of the equipment velocity per unit control command when h=20 (faint), h=100 (dashed), and h=100,000 (dotted). The solid line shows the case when no control is implemented. (d): Equipment velocity per primary excitation when the inner loop gains h=100 and different outer velocity feedback control gains are used: Z_D=0 (solid), Z_D=50 (faint), Z_D=100 (dashed), and Z_D=200 (dotted).*

The impedance of the equipment when the inner total transmitted force feedback control and the outer velocity feedback control are implemented is given by

$$Z = \frac{j\omega m_a k_a - \omega^2 m_a (c_a + hZ_D)}{k_a + j\omega c_a - \omega^2 m_a (1+h)} \tag{18}$$

which is plotted in Figure 14. It can be noted that, even when using low gains, the equipment impedance $q_t / v_e \cong Z_D$ past the first resonance frequency, which indicates that the overall system tends to a skyhook damper implementation. In conclusion, damping is added to the system in the form of the desired impedance Z_D, which is a positive real constant value that can be imposed by the designer.

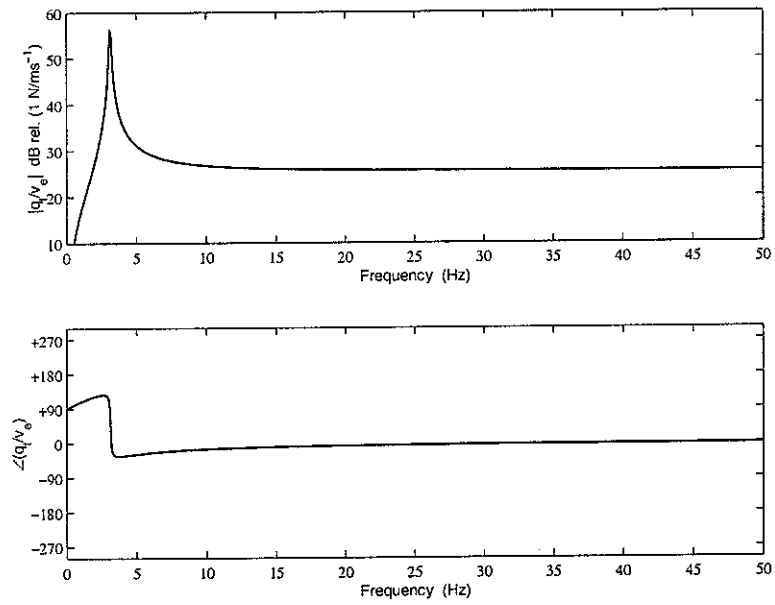

Figure 14 *Impedance of the equipment when the inner total transmitted force feedback control and the outer velocity feedback control are implemented. h=10 and Z_D=20.*

2.5 Outer Loop: Integrated Force and Velocity Feedback Control

Substituting equation (9) into (14), when the inner loop is based on an integrated feedback control strategy and the outer loop is a velocity feedback, the expression for the equipment velocity is given by

$$v_e = \frac{Y_e Z_m Y_b}{1 + Z_m(Y_e + Y_b + Y_e B_2 Y_b) + Y_e B_2} q_p + \frac{Y_e A_2 (1 + Y_b Z_m)}{1 + Z_m(Y_e + Y_b + Y_e B_2 Y_b) + Y_e B_2} f_c \quad (19)$$

Substituting (16) into (19) the equipment velocity per primary force is given by

$$v_e = \frac{Y_e Z_m Y_b}{1 + Z_m(Y_e + Y_b + Y_e B_2 Y_b) + Y_e B_2 + Y_e A_2 (1 + Y_b Z_m) Z_D} q_p \quad (20)$$

Figure 15(a) shows the equipment velocity per unit command signal for different values of the inner loop gain h. It can be noted that for high inner loop gains the first resonance is very damped, as expected. Figure 15(b) shows the equipment velocity per unit primary force for different values of the inner loop gain h. It is clear that the outer velocity feedback loop is needed in order to take energy away from the system. Figure 15(c) shows the Nyquist plot of v_e/f_c for different inner force feedback gains, which effectively determines the stability of the closed loop system once the outer velocity feedback control is implemented. When the inner force feedback gain h is increased, since the system with the inner control loop is unconditionally stable and very robust, the effect of increasing Z_D is good attenuation and unconditional stability. Figure 15(d) shows the equipment velocity per unit primary excitation. The effect of the inner force gain h=100 can be seen from the absence of the damped first resonance frequency. Performance-wise, it is shown that good vibration isolation conditions can be achieved, but high gains are needed. Also, at frequencies slightly higher than the equipment resonance frequency, enhancement, rather than attenuation, is experienced. This does not indicate good performance. In sum, from a stability point of view, the integrated force and velocity controller turns out to be very robust. This is mainly due to the fact that even under ideal conditions, the inner loop stability plot entirely lies on the positive x-axis semiplane. On the other hand, good performance can be achieved, but high outer loop gains are needed, therefore high energy is required.

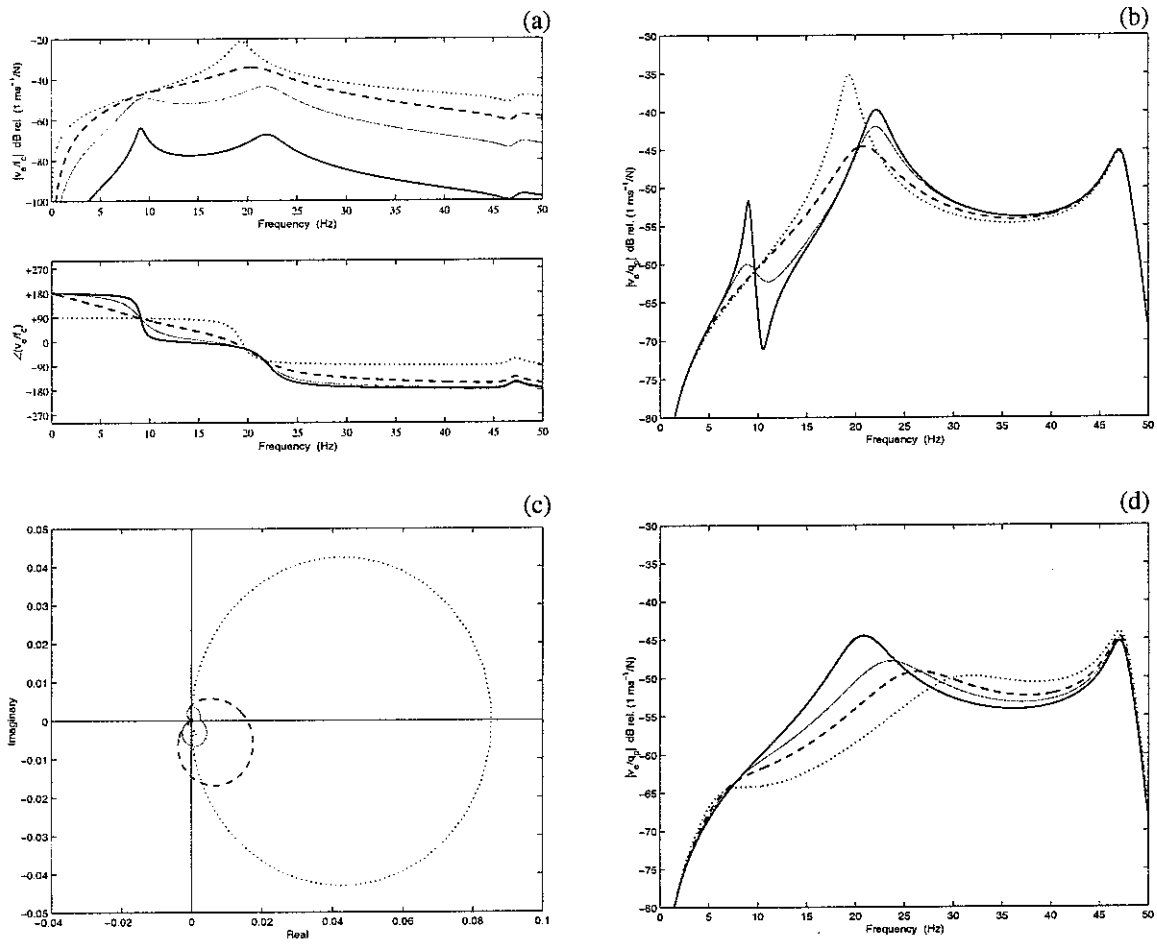

Figure 15 *(a): Equipment velocity per unit command signal when different inner loop gains h in $H(j\omega)=h/j\omega$ are used: h=1 (solid), h=20 (faint), h=100 (dashed), and h=100,000 (dotted). (b): Equipment velocity per unit primary force when h=0 (solid), h=20 (faint), h=100 (dashed), and h=100,000 (dotted). (c): Nyquist plot of the equipment velocity per unit control command when h=20 (faint), h=100 (dashed), and h=100,000 (dotted). The solid line shows the case when no control is implemented. (d): Equipment velocity per primary excitation when the inner loop gains h=100 and different outer velocity feedback control gains are used: Z_D=0 (solid), Z_D=50 (faint), Z_D=100 (dashed), and Z_D=200 (dotted).*

The impedance of the equipment when the inner and outer feedback control strategies are implemented is given by

$$Z = \frac{j\omega m_a (k_a + hZ_D) - \omega^2 m_a c_a}{k_a + j\omega c_a - \omega^2 m_a + j\omega m_a h} \tag{21}$$

which is plotted in Figure 16. It can be noted that, like in the previous case, the equipment impedance $q_t / v_e \cong Z_D$ past the first resonance frequency, which indicates that the overall system tends to a skyhook damper implementation. However, higher gains are needed to achieve this behaviour.

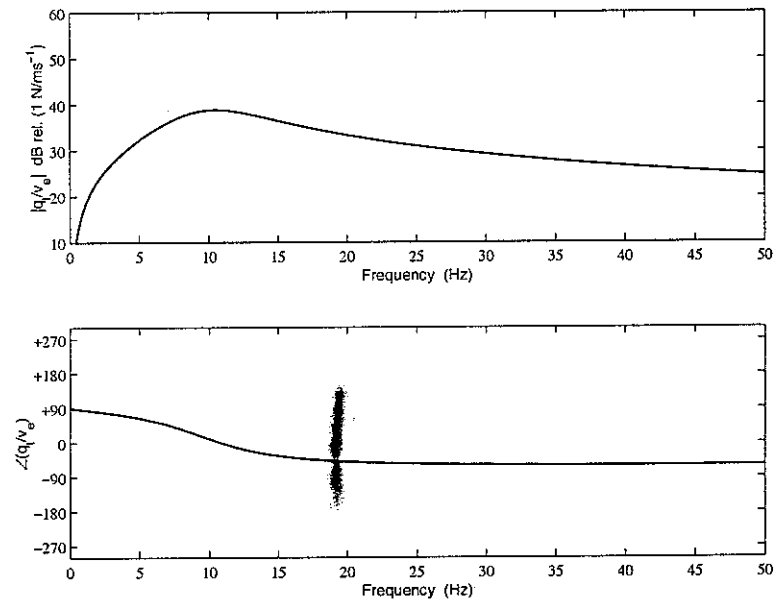

Figure 16 *Impedance of the equipment when the inner total transmitted force feedback control and the outer velocity feedback control are implemented. In particular, $H(j\omega)=h/j\omega$, . $h=50$ and $Z_D=20$.*

So far, it was shown that the force and velocity feedback control strategy is not robust, but it performs very well. On the other hand, the integrated force and velocity control strategy is more robust, but it requires higher gains in order to achieve comparable performance. In the next section a solution is presented which offers both robustness and good performance.

2.6 Outer Loop: Phase-lag and Velocity Feedback Control

Substituting equation (13) into (14), when the inner loop is based on a phase-lag compensator and the outer loop is a velocity feedback, the expression for the equipment velocity is given by

$$v_e = \frac{Y_e Z_m Y_b}{1 + Z_m(Y_e + Y_b + Y_e B_3 Y_b) + Y_e B_3} q_p + \frac{Y_e A_3 (1 + Y_b Z_m)}{1 + Z_m(Y_e + Y_b + Y_e B_3 Y_b) + Y_e B_3} f_c \quad (22)$$

Substituting (16) into (19) the equipment velocity per primary force is given by

$$v_e = \frac{Y_e Z_m Y_b}{1 + Z_m(Y_e + Y_b + Y_e B_3 Y_b) + Y_e B_3 + Y_e A_3 (1 + Y_b Z_m) Z_D} q_p \quad (23)$$

Figure 17(a) shows the equipment velocity per unit command signal for different values of the inner loop gain h. It can be noted that for high inner loop gains the first resonance is very damped, as expected. This is due to the fact that at low frequency the overall system behaves as if the integrated force controller was implemented. Figure 17(b) shows the equipment velocity per unit primary force for different values of the inner loop gain h. Even in this case, the outer velocity feedback loop is needed in order to take energy away from the system. Figure 17(c) shows the Nyquist plot of v_e/f_c for different inner force feedback gains. When the inner force feedback gain h is increased, since the system with the inner control loop is unconditionally stable and very robust, the effect of increasing Z_D is good attenuation and unconditional stability. Figure 17(d) shows the equipment velocity per unit primary excitation. The effect of the inner force gain h=100 can be seen from the absence of the damped first resonance frequency. Performance-wise, it is shown that good vibration isolation conditions can be achieved. This is due to the fact that at higher frequencies the overall system behaves as if a force feedback was implemented. Unlike the previous case, at frequencies slightly higher than the equipment resonance frequency attenuation is experienced. In sum, from a stability point of view, the system is very robust and it performs very well.

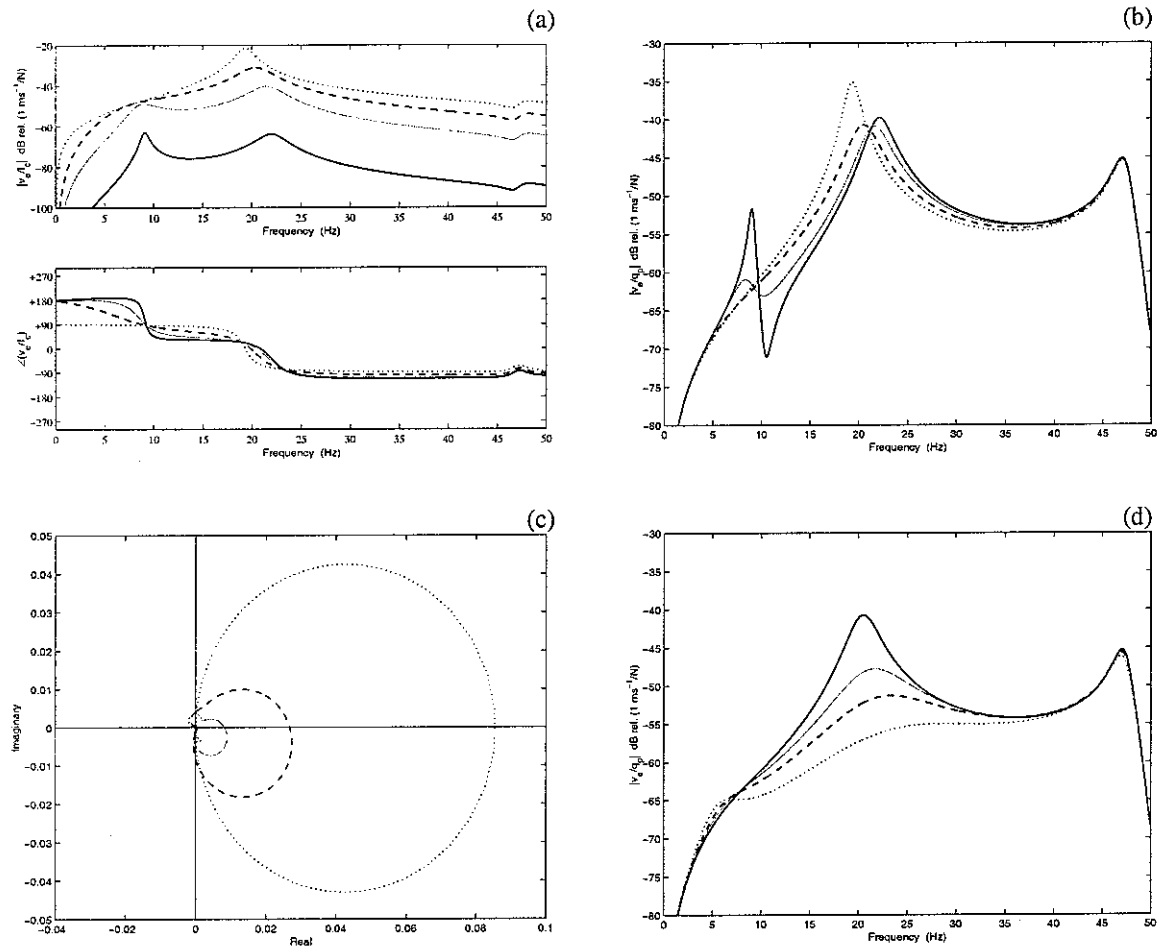

Figure 17 *(a): Equipment velocity per unit command signal when different inner loop gains h in the phase-lag compensator are used: h=1 (solid), h=20 (faint), h=100 (dashed), and h=100,000 (dotted). (b): Equipment velocity per unit primary force when h=0 (solid), h=20 (faint), h=100 (dashed), and h=100,000 (dotted). (c): Nyquist plot of the equipment velocity per unit control command when h=20 (faint), h=100 (dashed), and h=100,000 (dotted). The solid line shows the case when no control is implemented. (d): Equipment velocity per primary excitation when the inner loop gains h=100 and different outer velocity feedback control gains are used: Z_D=0 (solid), Z_D=50 (faint), Z_D=100 (dashed), and Z_D=200 (dotted).*

The impedance of the equipment when the inner and outer feedback control strategies are implemented is given by

$$Z = \frac{j\omega m_a(k_a + h'\omega_1 Z_D) - \omega^2 m_a(c_a + h'Z_D)}{k_a + j\omega c_a - \omega^2 m_a(1+h') + j\omega m_a h'\omega_1} \tag{24}$$

which is plotted in Figure 18. It can be noted that, like in the previous cases, the equipment impedance $q_t / v_e \cong Z_D$ past the first resonance frequency, which indicates that the overall system tends to a skyhook damper implementation. However, unlike the previous case, the tendency to a skyhook damper is more pronounced in this case ad this is due to the force-feedback-like behaviour (Figure 14) of the system at higher frequencies.

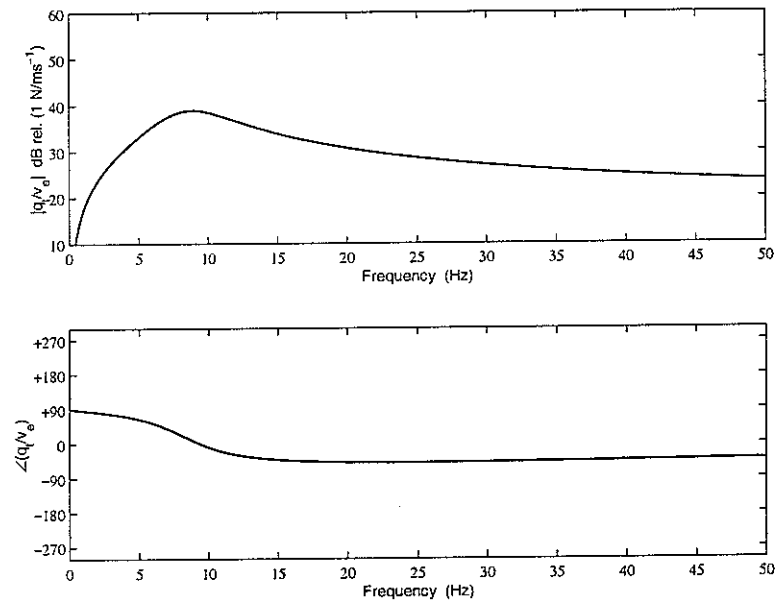

Figure 18 *Impedance of the equipment when the inner phase-lag control and the outer velocity feedback control are implemented. h=50 and Z_D=20.*

2.7 Actuator Requirement

The force requirement q_a for the three double feedback control schemes of interest has been investigated.

From the performance plots the inner and outer feedback gains (h and Z_D, respectively) have been chosen in order to determine if, given those gains which provide the desired performance of the closed loop system, reasonable force quantities can be provided by the inertial actuator. In other words, the following study will access if the inertial actuator can physically provide a certain amount of force which guarantees a desired performance of the overall system. The total transmitted force by the inertial actuator as a function of the control force (actuator requirement) q_a and the equipment velocity is given by

$$q_t = \frac{-\omega^2 m_a}{k_a + j\omega c_a - \omega^2 m_a} q_a - \frac{j\omega m_a k_a - \omega^2 m_a c_a}{k_a + j\omega c_a - \omega^2 m_a} v_e \tag{25}$$

which can be written in a more condensed expression as follows

$$q_t = Aq_a - Bv_e \tag{26}$$

The equipment velocity is given by

$$v_e = \frac{Y_e Z_m Y_b}{1 + Z_m(Y_e + Y_b)} q_p + \frac{Y_e(1 + Y_b Z_m)}{1 + Z_m(Y_e + Y_b)} q_t \tag{27}$$

Substituting equation (26) into (27), the equipment velocity can then be expressed as

$$v_e = \frac{Y_e Z_m Y_b}{1 + Z_m(Y_e + Y_b) + Y_e B(1 + Y_b Z_m)} q_p + \frac{Y_e A(1 + Y_b Z_m)}{1 + Z_m(Y_e + Y_b) + Y_e B(1 + Y_b Z_m)} q_a \tag{28}$$

In the double feedback control implementation q_a is given by

$$q_a = H(j\omega)(f_c - q_t) \tag{29}$$

where $H(j\omega)$ is specified depending on the inner loop feedback scheme. The outer loop controller is given by

$$f_c = -Z_D v_e \tag{30}$$

Substituting equation (30) into (29)

$$q_a = -H(j\omega)(Z_D v_e + q_t) \tag{31}$$

and then substituting equation (26) into (30)

$$q_a = \frac{H(j\omega)(B - Z_D)}{1 + H(j\omega)A} v_e \tag{32}$$

By substituting equation (28) into (32) the actuator requirement q_a per unit primary force q_p is obtained. For simplicity, H will be used instead of $H(j\omega)$, even though its meaning does not change.

$$q_a = \frac{H(j\omega)(B - Z_D)Y_e Z_m Y_b}{1 + Z_m(Y_e + Y_b) + Y_e B(1 + Y_b Z_m) + H(j\omega)A + H(j\omega)AZ_m(Y_e + Y_b) + H(j\omega)AY_e Z_D(1 + Y_b Z_m)} q_p \tag{33}$$

When the force and velocity feedback control scheme is implemented, $H(j\omega)=h$ (real positive). In this case q_a/q_p as a function of frequency is plotted in Figure 19. It can be noted that the actuator requirement depends not only on frequency, but also on the amount of primary excitation. This is not specific to a certain control scheme, but it holds in general. The effect of the inner force feedback controller can be noted by observing the frequency shift of the first resonance when h increases. At the same time, an increase in magnitude can be noted. This effect can be explained by comparing Figure 13(c) with Figure 19. For high gains the closed loop system gets closer to instability, therefore higher forces are required to control its behaviour.

The case where h = 100 and Z_D = 100 shows very good performance and in terms of actuator requirement the worst case scenario is experienced at the first resonance. At about 2 Hz, q_a/q_p = 20 dB = 10 N/N, so if q_p is a 1 N excitation, the actuator requirement is 10

N. This figure seems to be a lot if compared to the excitation, but it represents a worst case scenario and in any event it is physically achievable by small size commercial inertial actuators. As shown in Figure 19, the actuator requirement is much lower than the level of excitation.

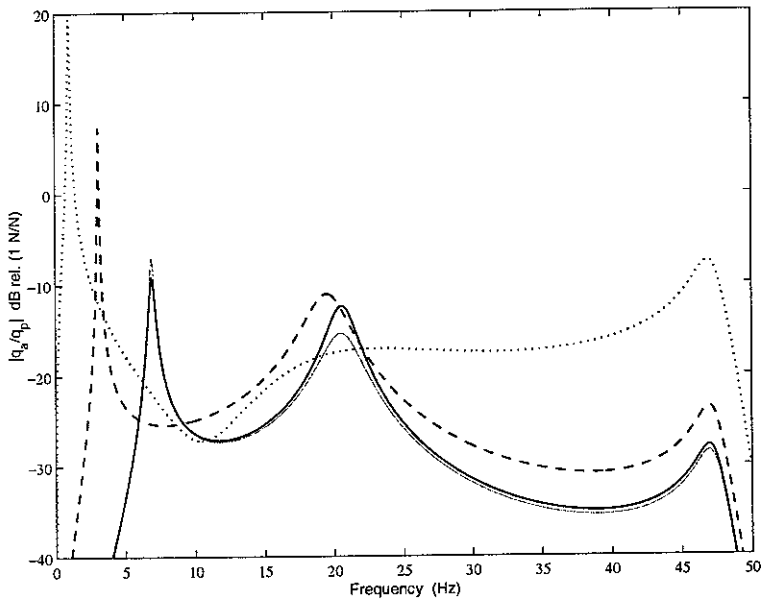

Figure 19 *Actuator requirement per unit primary excitation when the force and velocity feedback control strategy is implemented. Different control gains are used: h=1, Z_D=0 (solid); h=1, Z_D=10 (faint); h=10, Z_D=10 (dashed); h=100, Z_D=100 (dotted). In particular, this latter case shows very good performance, as plotted in Figure 13(d).*

Figure 20 shows q_a/q_p when $H(j\omega) = h\omega_0 / j\omega$ and $\omega_0 = 1$ rad/s. Even in this case the actuator force requirement is physically achievable. In particular, lower values of the force requirement are shown compared to the previous case, but it must be taken into account the fact that when integrated force and velocity is implemented and h and Z_D are both set to 100, the performance of the closed loop system is worse than the performance of the previous case when $h = Z_D = 100$. Also, since the closed loop system is more stable in the former case (Figure 15(c)), it is natural that it requires lower levels of force to control it. It can be shown that the actuator requirement per excitation force q_a/q_p is about 1 (on average) when h and Z_D are set in order to perform as efficiently as the $h = Z_D = 100$case when the force and velocity controller is implemented.

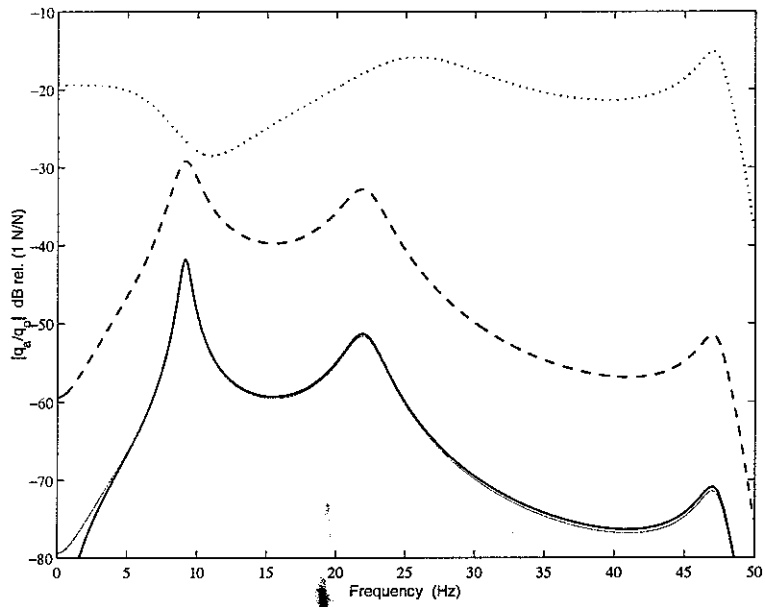

Figure 20 *Actuator requirement per unit primary excitation when the integrated force and velocity feedback control strategy is implemented. Different control gains are used: h=1, Z_D=0 (solid); h=1, Z_D=10 (faint); h=10, Z_D=10 (dashed); h=100, Z_D=100 (dotted).*

Figure 21 shows q_a/q_p when $H(j\omega) = h\frac{j\omega+\omega_1}{j\omega} = \frac{h}{\omega_1}\frac{j\omega+\omega_1}{j\omega}$ and $\omega_1 = 2\pi 20$ rad/s. The phase-lag compensator and velocity feedback controller shows a similar behaviour as the integrated force and velocity control scheme. This also confirms the usefulness of this solution. In fact, not only it can perform as efficiently as the force and velocity scheme, but also it can be as robust and in addition it requires low force levels as the integrated force and velocity case.

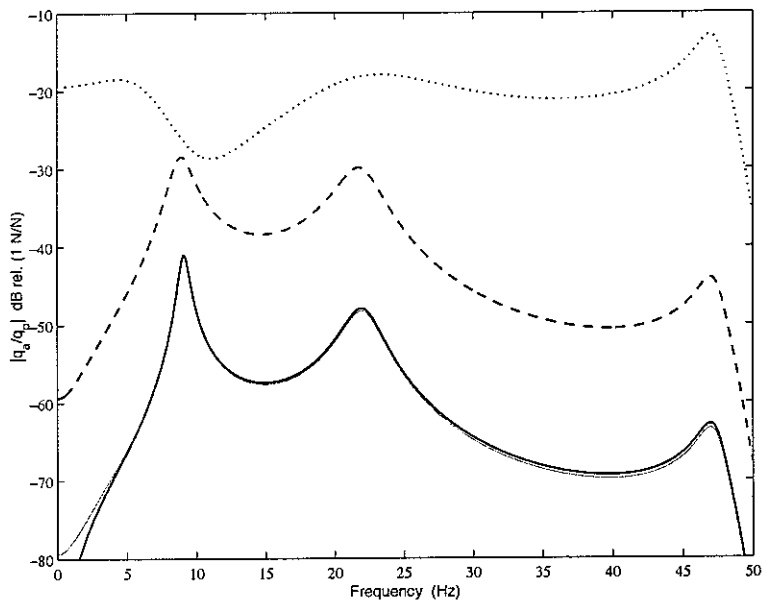

Figure 21 *Actuator requirement per unit primary excitation when a phase-lag compensator and velocity feedback control strategy are implemented. Different control gains are used: h=1, Z_D=0 (solid); h=1, Z_D=10 (faint); h=10, Z_D=10 (dashed); h=100, Z_D=100 (dotted).*

2.8 Conclusions

Inertial actuators do not need to react off a base structure, so they can be used as modules that can be directly installed on a vibrating structure. This feature makes them very attractive.

An analysis of different double feedback control strategies for active isolation using an inertial actuator was presented. Physical interpretation, feedback stability limits, performance, and robustness were considered for each case.

It was found that an internal feedback loop composed of a phase-lag compensator and an external loop composed of a velocity feedback provide a very good compromise between stability and performance of the system.

In this study it was assumed that the actuator resonance frequency was smaller than the equipment natural frequency. This is an important assumption and details can be found in Benassi *et al.* (2002a).

References

Ananthaganeshan, K. A., Brennan, M. J., and Elliott, S. J., 2001, "Low and High Frequency Instabilities in Feedback Control of a Vibrating Single Degree of Freedom System," ISVR Technical Report No. 870.

Benassi, L., Gardonio, P., and Elliott, S.J., 2002a, "Equipment Isolation of a SDOF System with an Inertial Actuator using Feedback Control Strategies – Part I: Theory," ISVR Technical Memorandom No. 883, University of Southampton.

Benassi, L., Gardonio, P., and Elliott, S.J., 2002b, "Equipment Isolation of a SDOF System with an Inertial Actuator using Feedback Control Strategies", *Proceedings of the ACTIVE 2002Conference, Southampton, U.K.*, 15-17 July 2002.

Crede, C. E., and Ruzicka, J. E., 1996, "Theory of Vibration Isolation," Chapter 30, C. M. Harris, ed., *Shock and Vibration Handbook*, McGraw Hill, New York.

Elliott, S. J., Serrand, M., and Gardonio, P., 2001, "Feedback Stability Limits for Active Isolation Systems with Reactive and Inertial Actuators," J. Vibration and Acoustics, Vol. 123, April 2001, pp. 250-261.

Gardonio, P., Elliott, S. J., and Pinnington, R. J., 1997a, "Active Isolation of Structural Vibration on a Multiple-Degree-of-Freedom System, Part I: the Dynamics of the System," J. Sound and Vibration, **207**, No. 1, pp. 61-93.

Gardonio, P., Elliott, S. J., and Pinnington, R. J., 1997b, "Active Isolation of Structural Vibration on a Multiple-Degree-of-Freedom System, Part II: Effectiveness of Active Control Strategies," J. Sound and Vibration, **207**, No. 1, pp. 95-121.

Appendix A. Complete Model Formulation

The system subject of the present study is composed of a vibrating base at the bottom, a piece of equipment mounted on top of the vibrating base through a passive mount, and an inertial actuator installed on the equipment. Figure 22 shows how the system is modelled and in particular it shows the sign convention. Each velocity or force is assumed to be positive in the direction indicated by the correspondent vector.

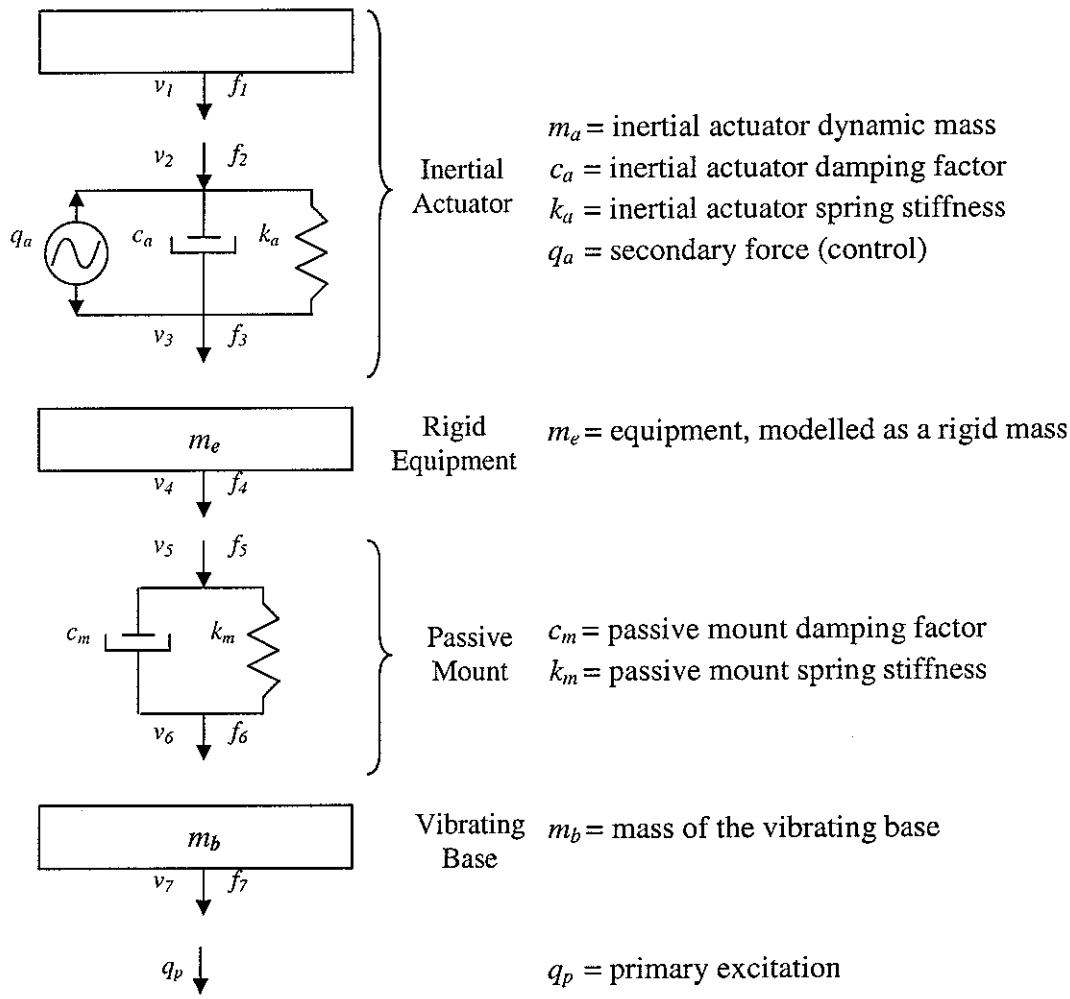

Figure 22 *Model of the system and sign convention.*

The equations that describe the system can be written as

$$v_1 = Y_{11} f_1 \tag{34}$$

$$v_1 = v_2 \tag{35}$$

$$f_1 + f_2 = 0 \tag{36}$$

$$\begin{Bmatrix} f_2 \\ f_3 \end{Bmatrix} = \begin{bmatrix} Z_{11}^a & Z_{12}^a \\ Z_{21}^a & Z_{22}^a \end{bmatrix} \begin{Bmatrix} v_2 \\ v_3 \end{Bmatrix} + \begin{bmatrix} -1 \\ 1 \end{bmatrix} q_a \tag{37}$$

$$v_3 = v_4 = v_5 \tag{38}$$

$$f_3 + f_4 + f_5 = 0 \tag{39}$$

$$v_4 = Y_{44} f_4 \tag{40}$$

$$\begin{Bmatrix} f_5 \\ f_6 \end{Bmatrix} = \begin{bmatrix} Z_{11}^m & Z_{12}^m \\ Z_{21}^m & Z_{22}^m \end{bmatrix} \begin{Bmatrix} v_5 \\ v_6 \end{Bmatrix} \tag{41}$$

$$v_6 = v_7 \tag{42}$$

$$f_6 + f_7 = 0 \tag{43}$$

$$v_7 = Y_{77}(f_7 + q_p) \tag{44}$$

where the mobilities and impedances are defined as

$$Y_{11} = \frac{1}{j\omega m_a}$$

$$Y_{44} = \frac{1}{j\omega m_e}$$

$$Y_{77} = plate - mobility$$

$$Z_{11}^a = Z_{22}^a = -Z_{12}^a = -Z_{21}^a = c_a + \frac{k_a}{j\omega}$$

$$Z_{11}^m = Z_{22}^m = -Z_{12}^m = -Z_{21}^m = c_m + \frac{k_m}{j\omega}$$

Equations (34), (40) and (44) can be grouped as

$$\begin{Bmatrix} v_1 \\ v_2 \\ v_3 \end{Bmatrix} = \begin{bmatrix} Y_{11} & 0 & 0 \\ 0 & Y_{44} & 0 \\ 0 & 0 & Y_{77} \end{bmatrix} \begin{Bmatrix} f_1 \\ f_2 \\ f_3 \end{Bmatrix} + \begin{bmatrix} 0 \\ 0 \\ Y_{77} \end{bmatrix} q_p \tag{45}$$

and rewritten as

$$\mathbf{v} = \mathbf{Y}\mathbf{f} + \mathbf{Y}_\mathbf{p} q_p \tag{46}$$

Considering equations (36), (39), (43), and (35), (38), (42), then equations (36), (37), (39), (41) and (43) can be grouped as

$$\begin{Bmatrix} f_1 \\ f_4 \\ f_7 \end{Bmatrix} = -\begin{bmatrix} Z_{11}^a & Z_{12}^a & 0 \\ Z_{21}^a & Z_{22}^a + Z_{11}^m & Z_{12}^m \\ 0 & Z_{21}^m & Z_{22}^m \end{bmatrix} \begin{Bmatrix} v_1 \\ v_4 \\ v_7 \end{Bmatrix} + \begin{bmatrix} 1 \\ -1 \\ 0 \end{bmatrix} q_a \tag{47}$$

and rewritten as

$$\mathbf{f} = -\mathbf{Z}\mathbf{v} + \mathbf{Z}_\mathbf{a} q_a \tag{48}$$

In sum, equations (46) and (48) represent a condensed form of the model of the system. Substituting equation (48) into (46)

$$\mathbf{v} = \left[I + \mathbf{Y}\mathbf{Z}\right]^{-1} \mathbf{Y}\mathbf{Z}_\mathbf{a} q_a + \left[I + \mathbf{Y}\mathbf{Z}\right]^{-1} \mathbf{Y}_\mathbf{p} q_p \tag{49}$$

and substituting equation (46) into (48)

$$\mathbf{f} = \left[I + \mathbf{Z}\mathbf{Y}\right]^{-1} \mathbf{Z}_\mathbf{a} q_a - \left[I + \mathbf{Z}\mathbf{Y}\right]^{-1} \mathbf{Z}\mathbf{Y}_\mathbf{p} q_p \tag{50}$$

From equations (49) and (50) it is possible to compute all the velocities and forces of interest within the system. Expanding equation (49), the analytical expressions for v_1, v_4 and v_7 can be obtained:

$$\begin{Bmatrix} v_1 \\ v_4 \\ v_7 \end{Bmatrix} = \frac{1}{D}\begin{bmatrix} (1+Y_{44}Z_{11}^m + Y_{77}Z_{22}^m)Y_{11} \\ -(1+Y_{77}Z_{22}^m)Y_{44} \\ Y_{77}Z_{21}^m Y_{44} \end{bmatrix} q_a + \frac{1}{D}\begin{bmatrix} Y_{11}Z_{12}^a Y_{44}Z_{12}^m Y_{77} \\ -(1+Y_{11}Z_{11}^a)Y_{44}Z_{12}^m Y_{77} \\ (1+Y_{11}Z_{11}^a + Y_{11}Z_{11}^a Y_{44}Z_{11}^m + Y_{44}Z_{11}^m + Y_{44}Z_{22}^a)Y_{77} \end{bmatrix} q_p \quad (51)$$

where

$$D = 1 + Y_{11}Z_{11}^a + Y_{11}Z_{11}^a Y_{44}Z_{11}^m + Y_{11}Z_{11}^a Y_{77}Z_{22}^m + Y_{44}(Z_{11}^m + Z_{22}^a) + Y_{44}Z_{22}^a Y_{77}Z_{22}^m + Y_{77}Z_{22}^m \quad (52)$$

Similarly, expanding equation (50), the analytical expressions for f_1, f_4 and f_7 can be obtained:

$$\begin{Bmatrix} f_1 \\ f_4 \\ f_7 \end{Bmatrix} = \frac{1}{D}\begin{bmatrix} 1+Y_{77}Z_{22}^m \\ -(1+Y_{77}Z_{22}^m) \\ Y_{44}Z_{12}^m \end{bmatrix} q_a + \frac{1}{D}\begin{bmatrix} Y_{11}Z_{12}^a Y_{44}Z_{12}^m Y_{77} \\ -(1+Y_{11}Z_{11}^a)Y_{44}Z_{12}^m Y_{77} \\ Y_{77}Z_{22}^m(1+Y_{11}Z_{11}^a + Y_{44}Z_{22}^a) \end{bmatrix} q_p \quad (53)$$

Equations (51) and (53) lead to identical expressions as those that were used in Benassi *et al.* (2002a,b) and also in this technical memorandum.

Appendix B. Choice of the Zero in the Phase-lag Compensator

Given the inner loop phase-lag compensator of the form $H(j\omega) = \frac{s+\omega_1}{s} = \frac{j\omega+\omega_1}{j\omega}$, where $\omega_1 = 2\pi f_1$, the choice of f_1 becomes of critical importance in order to assess a reasonable trade-off between stability of the overall system (especially at low frequency) and its performance. In fact, when f_1 is small, the system behaves similarly to the force and velocity implementation scheme. Under this condition, the system operates close to the unstable region. When f_1 is chosen to be high, an improvement, both stability-wise and performance-wise, occurs.

Figure 23(a) shows the Bode plot of $\frac{s+65.3}{s}$ for which f_1 =10.4 Hz. For comparison, Figure 23(b) shows the Bode plot of an ideal integrator of the form $\frac{1}{s} = \frac{1}{j\omega}$. This kind of integrator was used in the simulations discussed in the previous sections. It can be noted that thee is no phase recovery when the ideal integrator is implemented if compared to Figure 23(a). Also, the magnitude of the former compensator is much higher than the magnitude of the latter controller, which indicates that lower gains are needed in the former case to achieve the desired performance level.

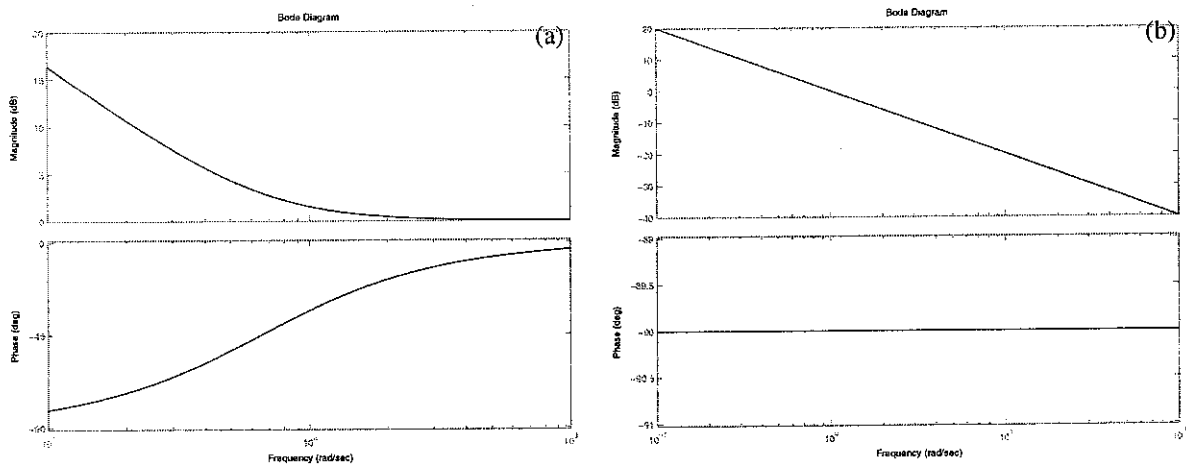

Figure 23 *Bode plot of* $\frac{s+65.3}{s}$ *(a), and Bode plot of* $\frac{1}{s}$ *(b).*

In particular applications, integrators are of the form $\frac{1}{1+\tau s} = \frac{1}{1+j\omega\tau}$, which implies that higher magnitude levels are achieved. In any event, the use of high gains, especially at high frequency, is necessary.

To summarize, the most important advantage of the phase-lag compensator is the fact that it enhances the stability of the system at low frequency and, thanks to its phase recovery, restores the original behaviour of the system at frequencies higher than f_1.

Figure 24 shows the Nyquist plot of $\det(\mathbf{I}+\mathbf{GH})$, where $\mathbf{G}$ and $\mathbf{H}$ are defined in Benassi (2002a), and where h and Z_D are set to 2 and 200, respectively, ad where f_1 is considered variable. As f_1 increases, at low frequency the Nyquist plot becomes steeper, which indicates a better stability margin. On the other hand, is f_1 is chosen to be large (Figure 24(b)) then stability problems are likely to happen at higher frequencies.

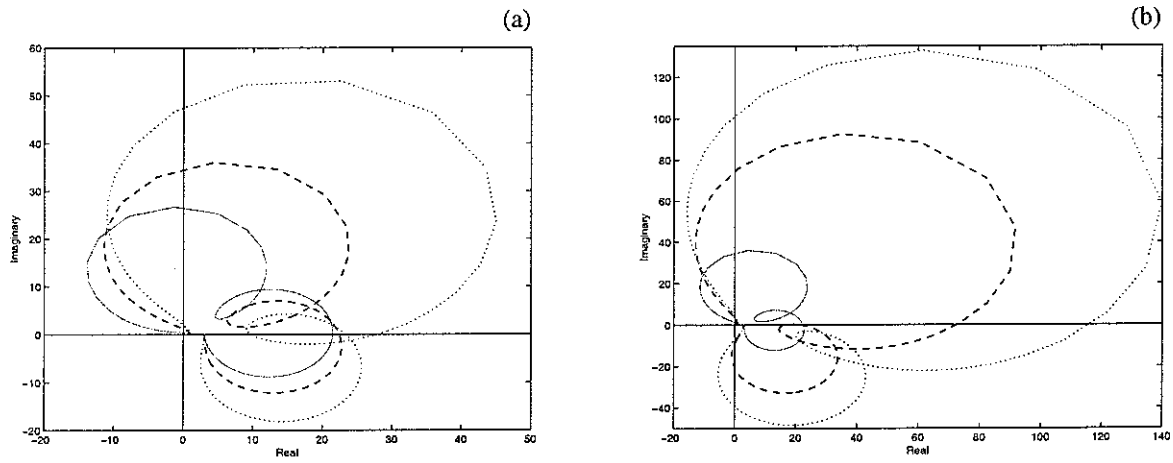

Figure 24 *Multichannel Nyquist plot of the determinant of* $(\mathbf{I}+\mathbf{G}(j\omega)\mathbf{H}(j\omega))$. *The plant is a vibration isolation system with an inertial actuator. The controller is the combination of a phase-lag compensator and velocity feedback. Different values of* f_1 *are used: (a)* f_1 *=4 Hz (solid),* f_1 *=10.4 Hz (dashed), and* f_1 *=22.5 Hz (dotted), and (b)* f_1 *=10.4 Hz (solid),* f_1 *=40 Hz (dashed), and* f_1 *=60 Hz (dotted).* ω *varies from 0 to* $+\infty$.

From a stability viewpoint, an accurate choice for the value f_1 would be in a region within the second resonance frequency of the system. In fact, when f_1 is close or lower then the first resonance, the system might become unstable if the electronic components are taken into account. However, if f_1 is greater than the second resonance frequency, instability at higher frequency (due to time delays in the electronic paths for example) may occur. An

important aspect of the above conclusion is that in the analysis a fixed set of gains h and Z_D was assumed, so it could be believed that by changing these gains the above conclusion might not hold any longer. This is not completely correct. In fact, an accurate design should consider both gains h and Z_D and f_1 as variables to be set in order to achieve the desired stability margin and performance characteristics.

As demonstrated below, the choice of f_1 has not a substantial impact on the performance characteristics of the system, but, as shown above, it is able to add margin to the stability at low frequency. On the contrary, as shown by Benassi *et al.* (2002a), an accurate selection of the gains leads to about 20 dB maximum attenuation (14 dB average) within a very remarkable frequency range.

Figure 25 shows the equipment velocity per unit primary force of the closed loop system when h and Z_D are set to 2 and 200, respectively, and when f_1 is allowed to vary. It can be noted that there is not a big difference performance-wise. One should remember that although a different choice of h and Z_D might lead to a better attenuation, the purpose of this analysis is to assess the influence of f_1.

An important aspect is depicted by the dashed line in Figure 25(a). When f_1 is lower than the first resonance frequency, an extra peak appears in the performance plot. This is also detectable in the rapid change in slope at low frequency in the correspondent Nyquist plot. This is physically due to the presence of the low frequency zero in the phase-lag compensator which becomes dominant at low frequency. Figure 25(b) shows the behaviour of the closed loop system for a different set of f_1. It can be noted that while there exists some improvement performance-wise when f_1 lies in the 12-20 Hz region, for higher values of f_1 the improvement is highly reduced and therefore the performance curve tends to a limit curve. This is due to a compensation between numerator and denominator in the v_e/q_p equation. From a physical point of view this can be explained by the fact that for high values of f_1 the behaviour of the first resonance frequencies is not affected by such a high frequency zero.

On the whole, not only for a stability point of view, but also from a performance point of view, f_1 should be chosen within the second resonance (mount-equipment) frequency range.

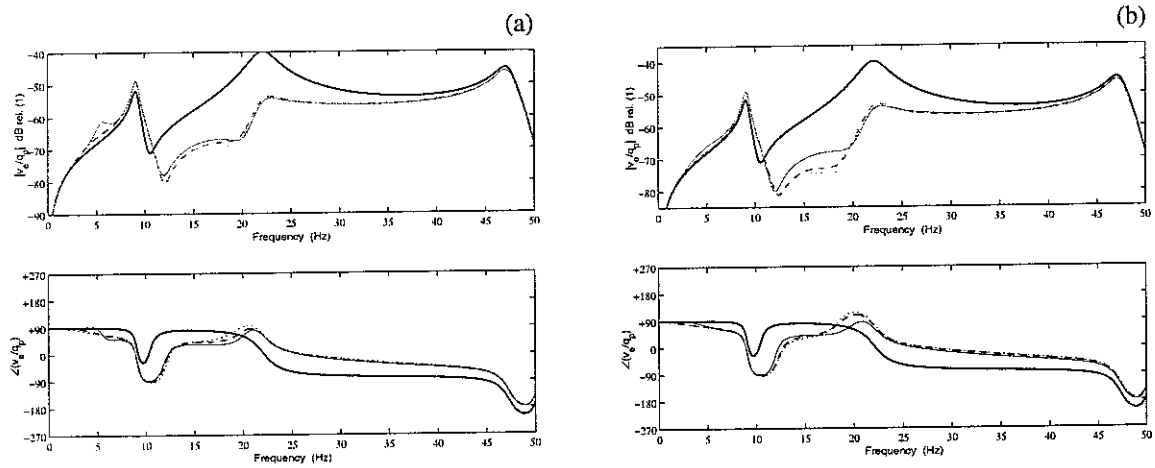

Figure 25 *Equipment velocity per unit primary excitation. Different values of f_1 are used: (a) f_1 =4 Hz (faint), f_1 =10.4 Hz (dashed), and f_1 =22.5 Hz (dotted), and (b) f_1 =10.4 Hz (faint), f_1 =40 Hz (dashed), and f_1 =60 Hz (dotted).The solid line shows the case where no control is implemented.*